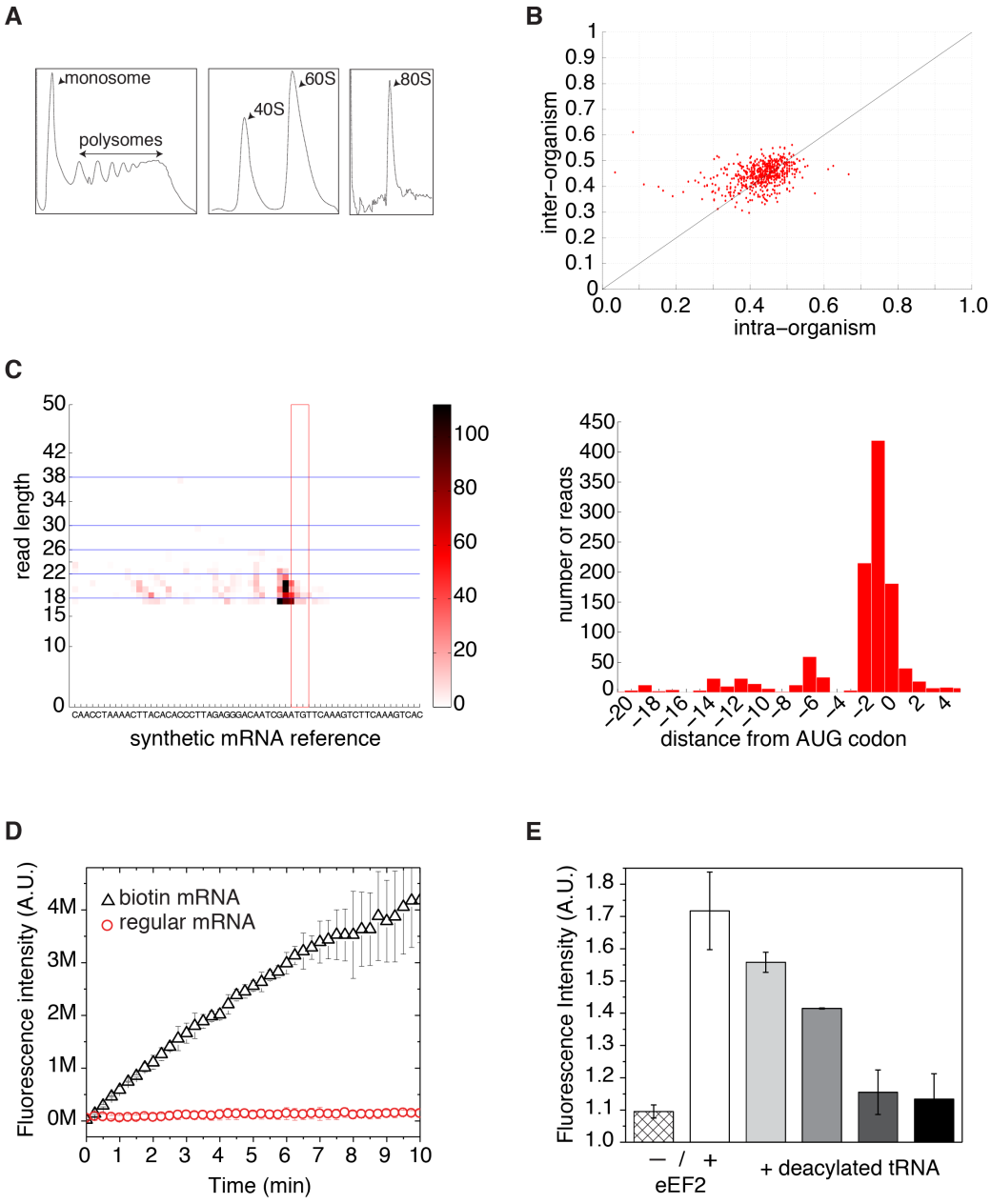

Figure S1, Related to Figure 1 | Purification and assembly of human ribosomes for bulk and single-molecule investigations. (A) Polyribosome fractions containing actively translating ribosomes were isolated from cultured human HEK293T cells by gradient density centrifugation (panel one). Polysomes were puromycin treated (pH-neutralized (pH 7.5; 2 mM) under high-salt (0.5 M KCl) conditions and the separated 40S and 60S subunits were isolated by sucrose gradient centrifugation (panel two). 80S ribosome complexes bearing mRNA and P-site Met-$tRNA_i^{Met}$ were assembled *in vitro* (Extended Experimental Procedures) and isolated by sucrose density gradient centrifugation (panel three). using this approach, the joining of large and small subunits was nearly quantitative. Each plot illustrates gradient fractionation from top to bottom

(left to right) while detecting absorbance at 254 nm. (B) Scatter plot showing the extent of sequence variations in tRNA outside of the anticodon (bases 34-37) within *E. coli* and *H. sapiens* (X axis) and between *E. coli* and *H. sapiens* (Y axis). This analysis shows that within its host, the ribosome processes tRNAs whose sequences display divergence of magnitude comparable to that between tRNAs from distantly related species. The ribosome mechanism must therefore be robust to the sequence divergence evidenced within the tRNA body. (C) Ribosome protected fragments obtained from the aforementioned 80S ICs using ribosome profiling procedures (Ingolia et al., 2012). Left panel: The 5' terminus of the fragment is indicated on the X-axis, with respect to the overall fragment length on the Y-axis. Ribosome protected fragments from the 80S IC were primarily 18-22 nucleotides in length and clustered around the AUG start codon. Right panel: Histogram showing the distribution of the 5' termini of ribosome protected fragments along the synthetic mRNA with respect to the AUG start codon. (D) 80S ICs programmed with Cy3-Met-tRNA^{Met} in the P site and mRNA containing a 5'-biotin moiety (Dharmacon) (1 nM; black tringles) bind rapidly and specifically via an engineered biotin-streptavidin interaction within polyethylene glycol-passivated quartz microfluidic chambers custom-designed for single-molecule imaging. 80S ICs lacking the 5'-biotin moiety (1 nM; red circles) do not appreciably bind to the engineered surfaces during the same time period. Using this approach, the surface density of ribosome complexes could be tuned according to the experimental demand: for puromycin experiments, a high ribosome complex density was employed; for single-molecule FRET experiments a low ribosome complex density was used to ensure that only one ribosome complex was present in a diffraction-limited area of the surface. As previously described (Blanchard et al., 2004), the biotin-dependent immobilization of dye-labeled tRNA ensures that only intact ribosome complexes are interrogated. (E) Processive translation assay monitoring the extent of (Cy3B)Phe-tRNA^{Phe} ternary complex de-quenching following incubation with 80S ICs. The left two bars represent biological triplicates in the absence (hatched) and presence (white bar) of eEF2. The four bars to the right represent biological triplicates of ligand-induced inhibition (from left) in the presence of eEF2 and 1nM (light gray), 10nM (medium gray), 100nM (dark gray) or 1 μM (black) deacylated tRNA purified from rabbit reticulocyte lysate.

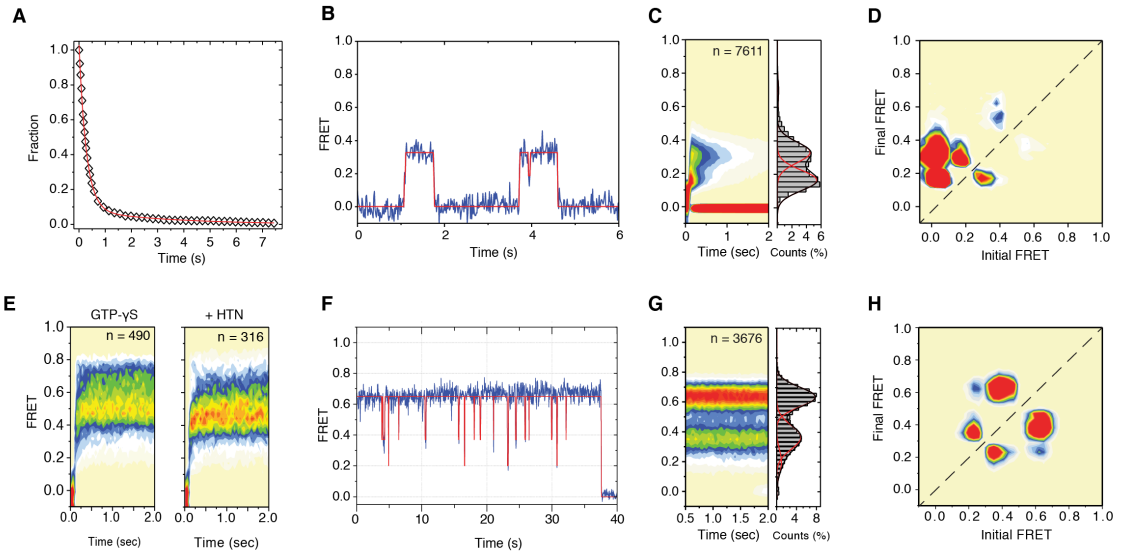

Figure S2, Related to Figure 2 | The human 80S ribosome is competent for aa-tRNA selection and exhibits pre-translocation complex dynamics that are distinct from those observed for the *E. coli* ribosome. (A) The process of tRNA selection was imaged under pre-steady state conditions by stopped-flow addition of an eEF1A•GTP•(Cy5)Phe-tRNA^{Phe} ternary complex (20 nM) to ribosomes containing (Cy3)Met-tRNA$_i^{Met}$ in the P-site. The binding of ternary complex to the 80S ribosome, marked by the appearance of FRET, exhibited a bimolecular rate constant (~170 μM^{-1} s^{-1}) consistent with a diffusion-limited macromolecular interaction (**Extended Experimental Procedures**). (B) A representative single-molecule trace showing non-productive interactions, typified by reversible binding events that predominantly exhibit intermediate-FRET (~0.33 FRET) configurations with infrequent transitions to low FRET (~0.17). (C) Population FRET histograms and (D) a transition density plot generated by combining all non-productive events reveal the distribution of FRET states observed and the frequency of transitions between states, respectively. Rare transitions to high FRET (~0.68) were also apparent. (E) The process of tRNA selection was imaged under pre-steady state conditions by stopped-flow addition of an eEF1A•GTP•(Cy5)Phe-tRNA^{Phe} ternary complex (20 nM) to ribosomes containing (Cy3)Met-tRNA$_i^{Met}$ in the P-site, with either the non-hydrolyzable GTP-analog GTPγS (left panel) or the drug HTN (10 μM) (right panel). Population FRET histograms were generated by combining all productive events to reveal the distribution of FRET states observed. (F) A representative single-molecule trace obtained from an *E.coli* 70S pre-translocation complex bearing (Cy3)tRNA^{Met} in the P site and (Cy5)Met-Phe-tRNA^{Phe} in the A site. As previously described (Munro et al., 2007), such complexes exhibit time-dependent transitions between low-, intermediate- and high-FRET states that correspond to two distinct hybrid tRNA positions and classical tRNA positions, respectively. (G) Population FRET histograms and (H) a transition density plot generated by combining all FRET data from individual molecules reveal the distribution of FRET states observed and the frequency of transitions between states, respectively. *E. coli* BL21 70S ribosome complexes were prepared and imaged using identical procedures and reagents as described for human 80S complexes.

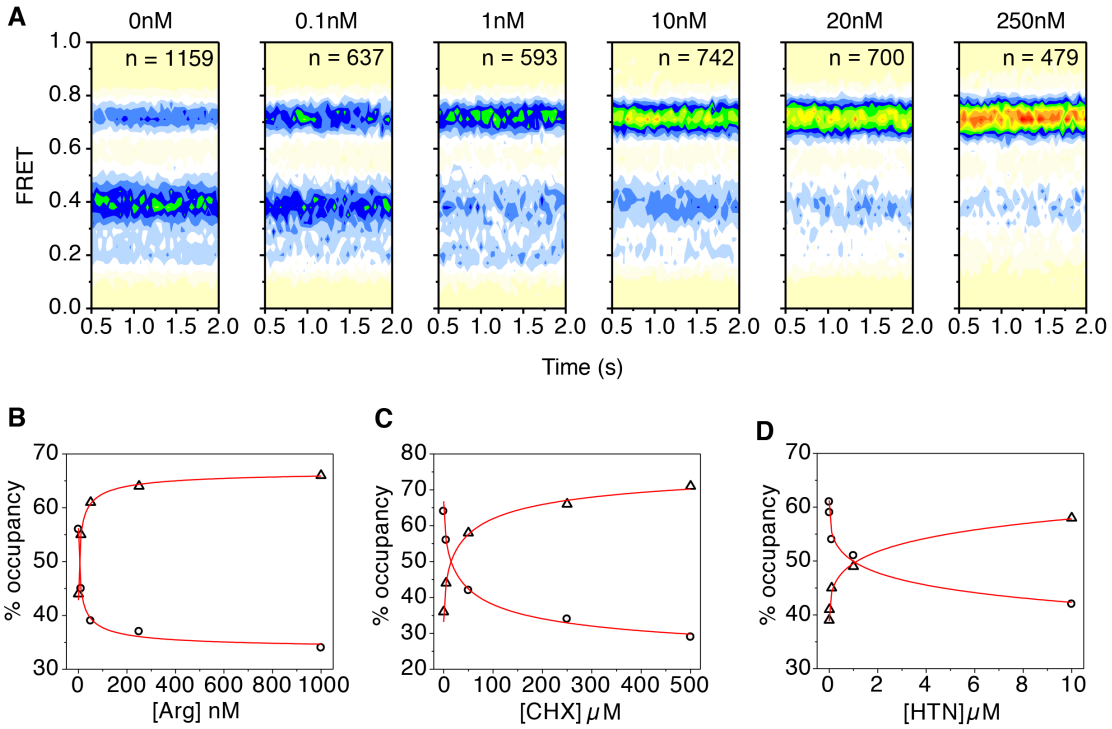

Figure S3, Related to Figure 3 | FRET state occupation can be quantified to determine binding affinity of ligands. (A) Population FRET histograms showing the impact of bulk deacylated-tRNA, purified from rabbit reticulocyte lysate (RRL), titrated into the empty E site while imaging the PRE complex. (B,C,D) Dose-response (EC_{50}) curves, based on the equation $y = A_1 + ((A_2 - A_1) / (1 + 10\text{^}(log_x0\text{-}x)p))$ where $EC_{50} = 10\text{^}log_x0$, were obtained by fitting changes in the relative population of specific FRET states exhibited by the human 80S PRE complex in response to ligand binding: (B) Addition of deacylated $tRNA^{Arg}$ stabilized the high- (~0.69) FRET configuration (triangles) in a concentration-dependent fashion, causing a corresponding decrease in lower-FRET configurations (circles). The estimated EC_{50} of this response was ~10 nM. (C) Addition of cycloheximide (CHX) stabilized the high- (~0.69) FRET (triangles) configuration in a concentration-dependent fashion, causing a corresponding decrease in lower-FRET configurations (circles); EC_{50} ~35μM (D) Addition of harringtonine (HTN) stabilized an intermediate- (~0.42) FRET configuration (triangles), and corresponding decrease in the combined occupancy in low-FRET and high-FRET states (circles); EC_{50} ~1μM. Fitting was performed using Origin (OriginLab Corporation).

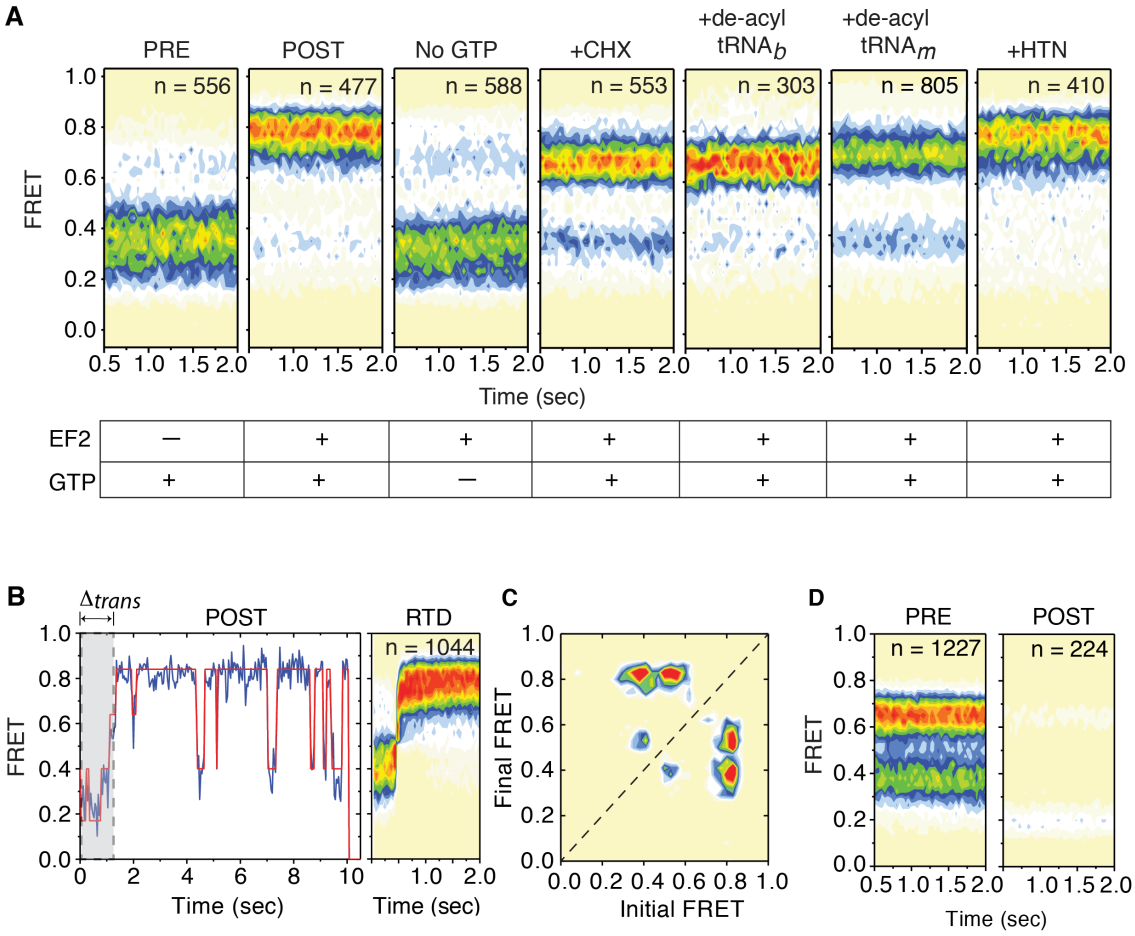

Figure S4, Related to Figure 4 | eEF2 catalyzed translocation of the 80S PRE complex. (A) Population FRET histograms demonstrate substrate translocation on the 80S PRE complex is eEF2 and GTP dependent. As shown in Figure 3, cycloheximide (CHX) and deacylated tRNA stabilize the classical state (~0.69 FRET). Here, CHX (500 µM) and both bacterial (tRNA$_b$) and mammalian (tRNA$_m$) deacylated tRNA (1 µM), isolated from *E. coli* and RRL, respectively, efficiently blocked translocation to the POST state (~0.82 FRET). Harringtonine (HTN) (10 µM) exhibited no net effect on the efficiency of translocation. (B) A representative single-molecule FRET trace (left panel) shows the time between injection of eEF2 (gray) and the transition to high FRET upon translocation. Post synchronization of individual FRET trajectories (**Extended Experimental Procedures**), obtained from pre-steady state eEF2•GTP translocation reactions to the point at which substrate translocation was achieved (arrival into a ~0.82 FRET state), produced population FRET histograms (right panel) demonstrating that translocation occurs within a single imaging frame from a predominantly low FRET (~0.37) configuration. (C) Transition density plot showing the observed FRET transitions exhibited by the POST ribosome complex. (D) Population FRET histograms of the PRE and POST state bacterial complexes reveal that the loss of Cy3 occurs rapidly from the POST state compared to human complexes (**Figure 4, 5A,B**) under the same experimental conditions.

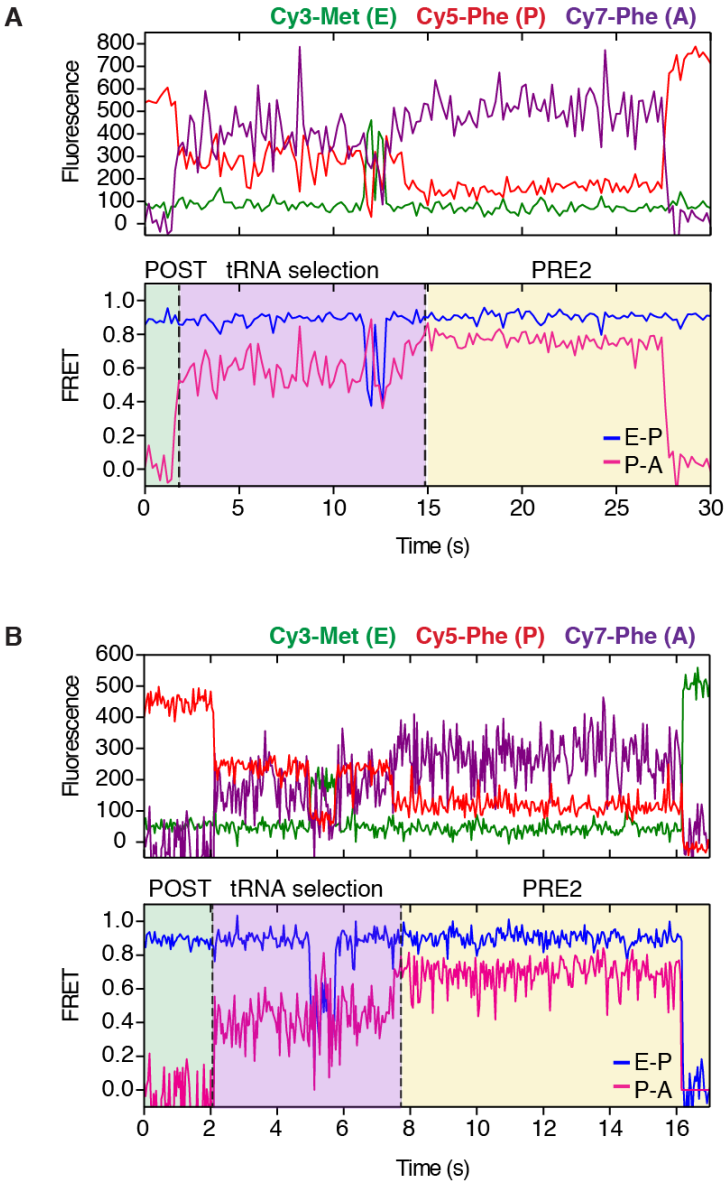

Figure S5, Related to Figure 5 | Three color smFRET reveals evidence of A site-E site allostery. (A) Stopped-flow delivery of an eEF1A•GTP•(Cy7)Phe-tRNA^{Phe} ternary complex (50 nM) to a POST complex containing (Cy3)tRNA$_i^{Met}$ in the E site and (Cy5)Met-Phe-tRNA^{Phe} in the P site. Time-dependent changes in FRET were monitored at 200 ms resolution. (B) The same experiment was repeated at 40 ms time-resolution.

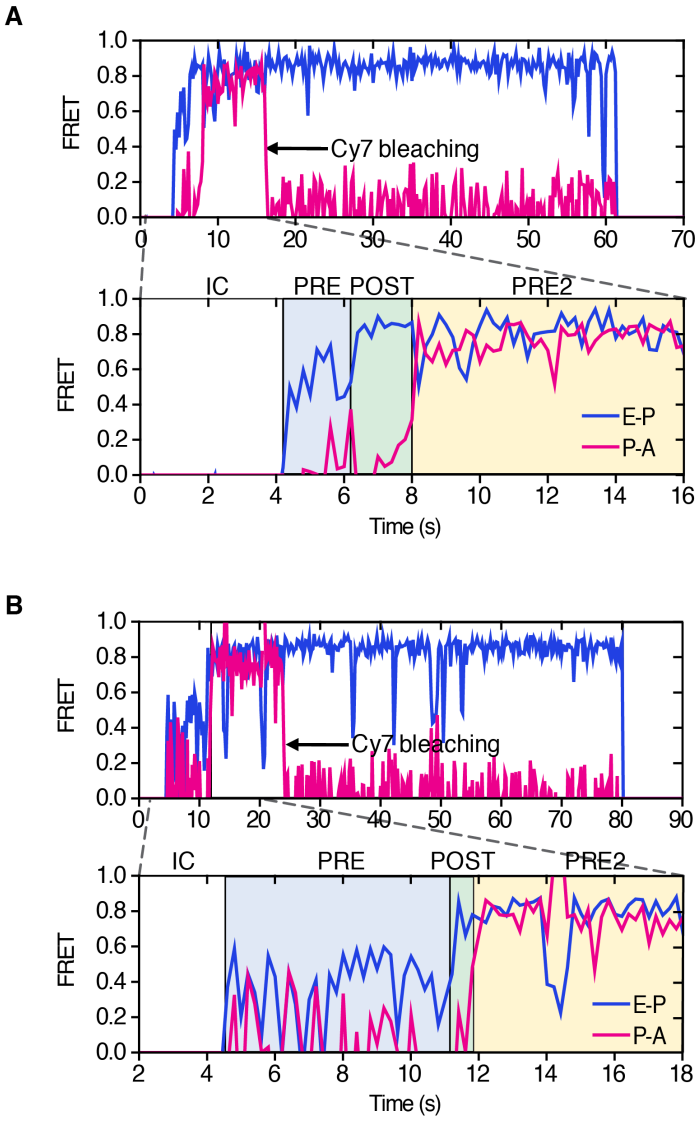

Figure S6, Related to Figure 6 | Stability and dynamics of the human ribosome during procesive translation. Stopped-flow delivery of (Cy5)Phe-tRNA^{Phe} and (Cy7)Phe-tRNA^{Phe} ternary complexes (10nM) to an 80S IC containing (Cy3)Met-tRNA$_i^{Met}$ in the P site. (A, B) Representative single-molecule traces of pre-steady state translation reactions (upper panels). Zoom (lower panels) demonstrates productive aa-tRNA selection and formation of a PRE complex (blue region), translocation to a POST state (green region), a second round of productive aa-tRNA selection (yellow region), and the presence of three independent, fluorescently-labeled tRNAs, concurrently bound to the ribosome, exhibiting dynamic motions. The area in white indicates the time occupied by the 80S IC before delivery of Cy5- and Cy7-labeled ternary complexes, eEF2 and GTP.

Large subunit			Small subunit		
Protein	**Uniprot ID**	**Score**	**Protein**	**Uniprot ID**	**Score**
uL3	P39023	2226.00	uS5	P15880	9822.92
uL4	P36578	3289.12	uS3	P23396	7835.83
uL18	P46777	4090.36	eS1	P61247	8340.49
eL6	Q02878	2564.05	eS4	P62701	5270.83
uL30	P18124	1843.56	uS7	P46782	7814.58
eL8	P62424	3158.82	eS6	P62753	5961.22
uL2	P62917	1819.09	eS7	P62081	4629.31
uL6	P32969	2744.04	eS8	P62241	6358.13
uL16	P27635	1196.34	uS4	P46781	3522.32
uL1	P62906	4262.90	eS10	P46783	6337.81
uL5	P62913	1141.64	uS17	P62280	4119.03
uL11	P30050	2183.44	eS12	P25398	6278.22
eL13	P26373	1777.59	uS15	P62277	3312.03
uL13	P40429	3147.17	uS11	P62263	4013.87
eL14	P50914	1930.49	uS19	P62277	599.3
eL15	P61313	2912.93	uS8	P62244	3682.97
uL22	P18621	1009.16	uS9	P62249	3213.93
eL18	Q07020	2280.96	eS17	P08708	3239.81
eL20	Q02543	1041.83	uS13	P62269	2789.62
eL19	J3QR09	1363.28	eS19	P39019	3043.92
eL21	P46778	666.50	uS10	P60866	1700.66
eL22	P35268	718.49	eS21	P63220	3015.45
uL14	P62829	3858.24	uS12	P62266	3650.72
uL23	P62750	2529.06	eS24	P62847	1974.48
eL24	P83731	1285.19	eS25	P62851	3088.17
uL24	P61254	599.29	eS26	P62854	1869.00
eL27	P61353	703.56	eS27	P42677	809.43
uL15	P46776	963.51	eS31	P62979	1619.15
eL28	P46779	818.12	eS28	P62857	1414.30
eL29	P47914	815.86	uS14	P62273	413.18
eL30	E5RI99	1212.97	eS30	P62861	549.41
eL31	P62899	507.68	uS2	C9J9K3	4298.98
eL32	D3YTB1	640.72	RACK1	P63244	10084.80
eL34	P49207	1060.57			
uL29	P42766	1043.39			
eL33	P18077	694.42			
eL36	Q9Y3U8	920.79			
eL42	P83881	543.86			
eL37	P61927	395.65			
eL43	P61513	3557.88			
eL38	P63173	1218.90			
eL39	P62891	66.53			
eL40	P62987	549.59			
eL41	P62945	not identified			
uL10	P05388	5626.43			

Table S1, Related to Figure 1 | List of ribosomal proteins identified by mass spectrometry. Protein names are listed with the nomenclature system used in Ban et al. 2014.

	k_{fast} (min^{-1})	A_{fast}	k_{slow} (min^{-1})	A_{slow}	*weighted average* $k_{apparent}$ (min^{-1})
80S IC	1.74	0.90	0.07	0.10	1.60
200 µM anisomycin	0.09	0.82	<0.01	0.18	0.08
PRE	0.91	0.65	0.08	0.35	0.62
POST	1.50	0.89	0.09	0.11	1.30
5 mM cycloheximide	0.67	0.47	0.06	0.53	0.35
200 µM sparsomycin	0.49	0.47	0.06	0.53	0.26
200 µM chloramphenicol	0.95	0.94	0.09	0.06	0.90

Table S2, Related to Figure 1 | Rates of PMN-release determined by loss of Cy3 fluorescence. The loss of fluorescence from surface-immobilized 80S ribosome complexes bearing Cy3-Met-$tRNA^{Met}$ in the P site upon addition of pH-neutralized (pH 7.5) puromycin (2 mM) was monitored over time (10 min) under low intensity illumination. The apparent rate of fluorescence loss reflects the sum of the bimolecular rate constant between puromycin and the 80S complex, the rate of peptide bond formation and the rate of Cy3-peptidyl-puromycin release from the ribosome and the evanescent field generated by total internal reflection. Control experiments showed that the photobleaching rate of the 80S human ribosome lacking A-site tRNA (80S IC) was approximately 0.014 min^{-1} and thus contributed negligibly to the apparent rate of puromycin reaction. Correspondingly, all data were fit to a double exponential decay processes using the equation $y = A_{fast}*\exp(-x/t_{fast}) + A_{slow}*\exp(-x/t_{slow})$. Decay rates were then calculated as 1/t. Fitting was performed using Origin (OriginLab Corporation). The apparent rate of puromycin reaction for the 80S empty A-site complex was approximately 2.5-times slower than observed for bacterial ribosomes under similar conditions (Munro et al., 2007).

EXTENDED EXPERIMENTAL PROCEDURES:

Growing and Harvesting Human Cells

Human HEK293T cells were maintained in Dulbecco's modified Eagle's medium (DMEM) with high glucose (Gibco® from Invitrogen), 10% fetal bovine serum (FBS) and streptomycin/penicillin antibiotics (Life Technologies). At 75% confluency, cells were treated with 100 µg/mL cycloheximide for 30 minutes and then harvested by trypsin digest and centrifugation. Cell pellets were frozen in liquid nitrogen and stored at -80°C until cell lysis.

Purification of 40S and 60S ribosomal subunits

Preparation of small (40S) and large (60S) human ribosomal subunits, free of endogenous tRNAs and mRNAs, was adapted from (Bommer et al., 1997). Specific deviations implemented for the purification of polysome fractions from human tissue culture are described here. Cell pellets were resuspended in lysis buffer (20 mM Tris HCl, pH 7.5, 2.5 mM $MgCl_2$, 10 mM KCl and 1 mM freshly prepared DTT) with RNAse inhibitor RNAse Out™ (Invitrogen), EDTA free Halt™ Protease Inhibitor (Thermo Scientific) and cycloheximide (Sigma) at 100 µg/mL (~350 µM). The solution was incubated on ice for 10 minutes before centrifugation in a Microfuge™ 22R Refrigerated Centrifuge (Beckman Coulter) at 14,000 rpm for 10 minutes at 4°C to pellet cell debris. The supernatant was loaded onto pre-cooled 10-50% sucrose density gradients and spun at 35,000 rpm for 3 hours at 4°C in an Optima L-100 XP ultracentrifuge (Beckman Coulter). The gradients were then fractionated using a BR-186-1 Fractionator and a UA-6 UV/Vis detector (Teledyne ISCO). Fractions corresponding to polysomes were collected and subsequently pelleted and dissociated into subunits according to (Bommer et al., 1997). Pelleted subunits were resuspended with storage buffer (30 mM HEPES pH 7.5, 15 mM $MgCl_2$, 50 mM NH_4Cl, 2 mM Spermidine, 5 mM Putrescine, 1 mM DTT and 6% sucrose) for stable, long-term storage in liquid nitrogen.

Mass Spectrometry analysis of ribosomal subunits

Human 40S and 60S subunits were prepared as described above. Samples were denatured with urea, reduced with DTT and alkylated using iodoacetamide followed by overnight digestion with trypsin at 37° C. Resulting peptides were purified using C18 StageTips. Samples were analyzed using nano-flow HPLC at a flow rate of 150 µl/min coupled to a QExactive mass spectrometer using a gradient of 120 min. with an MS and MSMS resolution of 70,000 and 17,500 respectively, using Higher Energy Collision Dissociation fragmentation. The top 20 most intense peaks were picked for fragmentation for each scan. Data were extracted and queried against UniProt Human using Proteome Discoverer and MASCOT. Identified peptides were filtered using 1% False Discovery Rate (FDR) and Percolator (Käll et al., 2007). Potential common Fetal Bovine Serum and human contaminants were included in the database (Bunkenborg et al., 2010).

Preparation of native and fluorescently-labeled tRNAs.

E.coli $tRNA^{Met}$ and $tRNA^{Phe}$ were purified as previously described (Dunkle et al., 2011; Wang et al., 2011). $tRNA^{Arg}$ from MRE600 was purchased from Chemical Block. Aminoacylation and fluorescent labeling of tRNAs ($tRNA_i^{Met}$ at $4sU^8$ and $tRNA^{Phe}$ at acp^3 U47 positions) were performed following established protocols (Blanchard et al., 2004). *E. coli* tRNA were utilized in this study in order to capitalize on prior validation of the functionality of labeled tRNA and to tether findings to previous studies on bacterial and rabbit ribosomes using the same labeled tRNAs (Blanchard et al., 2004; Budkevich et al., 2011; Geggier et al., 2010; Wang et al., 2011).

Transfer RNA species from each kingdom of life exhibit conserved secondary and tertiary structures as well as intra- and inter-species sequence variation. The extent of tRNA sequence variation within and between organisms is such that tRNAs within a single organism (eg. *E. coli* or *H. sapiens*) are as varied as they are between species (see **Figure S1B**). To perform this analysis we considered sets of tRNA sequences, each pertaining to a distinct anticodon in a different organism. tRNA sequence divergence outside of the anticodon region between two sets of tRNA sequences is defined to be the median divergence amongst all pairwise comparisons of tRNAs coming from two distinct sets. Two cases are considered: the sets of tRNA transcripts are restricted to both be from the same organism (*H. sapien* or *E. coli*) (X-axis*)*; the sets of tRNA transcripts are from different organisms (*H. sapien* vs. *E. coli*) (Y-axis). For example, the intra-organism tRNA divergence between tRNA species identified by AUG and ACA anticodons is obtained by computing the pairwise sequence divergence for each tRNA transcript bearing an AUG anticodon against each tRNA bearing an ACA anticodon, for *H. sapien* and *E. coli*, separately. The intra-organism tRNA divergence between anticodons AUG and ACA is defined as the median of these two combined lists of sequence divergences. The inter-organism sequence divergence is similar, except that pairs come from *different* species. Thus, the inter-organism tRNA divergence between anti-codons AUG and ACA is the median of sequence divergences of all pairs of *H. sapien* tRNA bearing AUG anticodons *vs. E.coli* tRNAs bearing ACA anticodons, and all pairs of *E. coli* tRNA bearing AUG anticodons *vs. H. sapien* tRNA bearing ACA anticodons. As this analysis stipulates that the ribosome mechanism is robust to variations in tRNA sequence, we employed highly purified and active tRNAs from *E. coli* which are fully functional in aminoacylation, ternary complex formation, tRNA selection, translocation and processive translation.

In vitro-reconstitution of 80S Initiation Complex

80S initiation complexes (ICs) were assembled following a procedure that bypasses the need for exogenous initiation factors (Burgess and Mach, 1971). Purified 40S subunits were mixed with an equal volume of 80S Association Buffer (30 mM Hepes pH 7.5, 5 mM $MgCl_2$, 50 mM NH_4Cl, 2 mM Spermidine, 5 mM Putrescine, 1 mM DTT) and then heat activated at 42°C for 5 minutes. Four-fold excess of mRNA***** with the sequence 5'-CAA CCU AAA ACU UAC ACA CCC UUA GAG GGA CAA UCG AUG UUC AAA GUC UUC AAA GUC AUC-3' (Dharmacon) (henceforth described as *MKF* mRNA) or 5'-CAA CCU AAA ACU UAC ACA CCC UUA GAG GGA CAA UCG AUG UUU UUU UUU UUU UUU UUU UUU-3' (Dharmacon) (henceforth described as *MFF* mRNA) was added, heated to 37°C for 10 minutes and subsequently cooled on ice. To this mixture, a two-fold excess of fluorescently-labeled or unlabeled Met-$tRNA_i^{Met}$ (prepared as described in Blanchard et al., 2004) was added and the reaction was heated and cooled, as above. At this time, equimolar amounts of 60S subunits were heat activated at 42°C for 5 minutes. The 60S subunits were then added to the mixture of 40S/tRNA/mRNA. After an additional heating and cooling cycle, the $MgCl_2$ concentration of the reaction was raised to 15 mM and the mixture remained on ice for 5 minutes. It was then loaded on a 10-30% sucrose gradient in 80S Association Buffer and was ultracentrifuged in a Beckman SW41 rotor at 35,000 rpm for 1.5 hours at 4°C before fractionation. The peak corresponding to 80S complexes was collected and aliquoted prior to storage in liquid nitrogen. *****For surface-immobilization experiments, the mRNA is first hybridized to a double-stranded biotinylated DNA linker with the sequence 5'-GTA AGT TTT AGG TTG CCC CCC TTT TTT TTT TTT TTT TTT TTT TTT TTT TTT-3'/ 3'-AAA AAA AAA AAA AAA AAA AAA AAA AAA AAA-5'.

Formation of the EF•GTP•aa-tRNA ternary complex.

Aminoacylated (aa)-tRNAs ($tRNA^{Phe}$, $tRNA^{Met}$) were first generated as previously described (Blanchard et al., 2004) and mixed with 1 mM GTP, 6 mM phosphoenolpyruvate, 12 units/mL pyruvate kinase and 12 units/mL myokinase. A two-fold excess of eEF1A isolated from rabbit liver, which bears 100% sequence identity with human eEF1A (a kind gift from Dr. Christian Spahn (Budkevich et al. Cell, 2014)) or EF-Tu, the bacterial homologue of eEF1A (Burnett et al., 2014) was then added and the mixture was incubated at 37°C for 5 minutes to form the ternary complex.

Bulk translation activity assays.

Human 80S ribosome complexes were assembled *in vitro* as described above on a synthetic MFK mRNA with unlabeled Met-$tRNA_i^{Met}$ in the P site. Bulk fluorescence-based assays were performed in a Tecan Infinite M1000 Pro fluorescence plate reader in 384-well flat bottom plates. Quenched ternary complex ((Cy5Q)EF-Tu•GTP•(Cy3B)Phe-$tRNA^{Phe}$)) was formed according to published protocols (Burnett et al., 2014). As bacterial EF-Tu can function in concert with eEF2 and 80S ribosomes in peptide chain elongation (Grasmuk et al., 1977; Krisko et al., 1969), single-turnover and processive translation reactions were monitored via the de-quenching process that results from codon-dependent release of Cy3B-tRNA from EF-Tu as it releases from the ribosome. Cy3B fluorescence only increased when ribosome complexes were properly initiated at the AUG start codon as the subsequent codon in the A site is UUC (Phe). Ribosomes initiated such that when they were programmed with near- or non-cognate mRNA codons or lacking P-site tRNA, they were unable to de-quench ternary complex (**Figure 1A**).

Single-turnover, fraction active assays were performed by adding increasing concentrations of *in vitro* reconstituted 80S ICs to a reaction mixture containing fixed concentrations of quenched ternary complex in a defined buffer containing polyamines (30 mM HEPES pH 7.5, 5 mM $MgCl_2$, 50 mM NH_4Cl, 2 mM spermidine, 5 mM putrescine, 1 mM DTT) that supports processive translation. Increased Cy3B fluorescence, accompanying the accommodation of (Cy3B)Phe-$tRNA^{Phe}$ into the A site, was monitored in real time by exciting the Cy3B fluorophore at 532 nM and detecting the increase in fluorescence emission at 575 nm.

Processive translation reactions were performed by adding 80S ICs (20 nM), assembled as described above on a synthetic MFF mRNA to a reaction mixture containing quenched ternary complex ((Cy5Q)EF-Tu•GTP•(Cy3B)Phe-$tRNA^{Phe}$) (100 nM) and eEF2 (100 nM) isolated from rabbit reticulocyte lysate (a kind gift from Dr. Christian Spahn), which bears approximately 98% sequence identity with human eEF2 (Genbank). The time-dependent increase in Cy3B fluorescence resulting from (Cy3B)Phe-$tRNA^{Phe}$ entry into the A site of the ribosome was monitored in real time as described above. As expected, processive translation was inhibited by the addition of cycloheximide (Sigma) (5 μM, 50 μM, 500 μM), harringtonine (a kind gift from Dr. Daniel Wilson) (0.1 μM, 1 μM, 10 μM), or de-acylated $tRNA^{Arg}$ (ChemBlock) (0.02 μM, 0.2 μM, 2 μM).

Ribosome profiling

Ribosome profiling procedures were adapted from Ingolia et al., 2012. Human ribosome 80S initiation complexes on synthetic mRNA were prepared following the above protocol, with the following adaptations, and supplemented with 5-fold excess of free ribosomal subunits as carrier RNA. This mixture was suspended in 300 μL of lysis buffer (20 mM Tris – HCl pH 7.4, 150 mM NaCl, 5 mM $MgCl_2$, 1 mM DTT, 350 μM cycloheximide, 1% Triton–X and Turbo Dnase (25 U mL^{-1}) (Life Technologies)). Complexes were digested using 750 Units of RNase I (Life

Technologies) for 15 minutes at room temperature. The digestion reaction was stopped by addition of 200 Units of Superase.In (Life Technologies).

Digested ribosome complexes were transferred into a polycarbonate ultracentrifuge tube (13 mm x 51 mm, Beckman 349622) and underlayed with 900 µL of a 1 M sucrose cushion (1 M sucrose, 20 mM Tris-Cl, 0.5 M NH_4Cl, 20 mM $MgCl_2$, 1 mM DTT and 500 µM cycloheximide). Ribosome pellets were collected using an Optima TLX ultra centrifuge (Beckman 361454) and TLA 100.3 rotor (Beckman 349481) with centrifugation at 78,000 RPM for 4 hours at 4°C and re-suspended in 350 µL of dissociation buffer (0.5 M KCl, 1 mM Puromycin, 35 Units of Superase.In, PBS pH 7.4). Sub-units were subsequently pelleted for 2 hours at 90,000 RPM at 4°C. The supernatant was recovered and RNA was isolated using a Qiagen RNeasy Kit according to the manufacturer's instructions.

The ribosome protected fragment library was constructed according to previously published protocols (Ingolia et al., 2012) and sequenced on an Illumina HiSeq 2500 machine. Files were treated according to published protocols (Ingolia et al., 2012). A synthetic genome was generated using the mRNA sequence 5'-CAA CCU AAA ACU UAC ACA CCC UUA GAG GGA CAA UCG AUG UUC AAA GUC UUC AAA GUC AUC-3'. Ribosome profiling reads were trimmed for adaptor sequence (CTGTAGGCACCATCAAT) and the first base was clipped. The reads were then aligned against human and mouse rRNA sequences (for human: NR_003286.2, NR_003287.2, NR_003285.2, NR_023379.1; for mouse: NR_003278.3, NR_003279.1, NR_003280.2, NR_030686.1) with BWA (Li & Durbin 2009). Reads that failed to map to the rRNA sequences were then mapped against the synthetic mRNA sequence. Output alignment data were visualized using IGV v.2.3.39 (Robinson et al., 2011).

Single-molecule FRET analysis

Single molecule fluorescence data were analyzed as previously described (Budkevich et al., 2011; Munro et al., 2007) using custom software written in MATLAB. Molecules were detected as peaks of fluorescence intensity in a summed, aligned, and background-subtracted image of all fluorescence channels. Fluorescence intensity associated with each peak was collected by summing the brightest pixels in a local neighborhood around each peak in each channel. Background levels in each channel were subtracted as determined after donor photobleaching. Fluorescence bleed-through from Cy3 to Cy5 and Cy5 to Cy7 channels was corrected by subtracting a set fraction of Cy3 intensity from Cy5 and Cy5 intensity from Cy7. The fluorescence intensity signals from each channel were scaled so that the apparent brightness of each fluorophore was equal (Ha et al., 1999).

Single-molecule FRET traces from multiple movies were combined and a subset were selected using fixed criteria to exclude traces with low signal-to-background noise ratios or short FRET lifetimes. Traces were rejected if they exhibited any of the following characteristics indicative of experiment-specific artifacts: high background, correlated changes in donor and acceptor signals, photobleaching indicating the presence of multiple donors or intermittent dark states (blinking) of the donor. As previously described (Munro et al., 2007), individual FRET trajectories were idealized by hidden Markov modeling using the segmental k-means algorithm implemented within the QuB software package (Qin et al., 2004). The quality and robustness of these idealized procedures were examined using Transition Density Plots (TDPs), which provide a convenient representation of all FRET transitions identified in the idealized data by plotting as a single data point the average FRET value observed prior to each transition (X-axis; Initial FRET) and the average FRET value observed at the end of each transition (Y-axis; Final FRET) as originally described (McKinney et al., 2006). Time-averaged occupancies in each FRET state were calculated from the total dwell times observed divided by the total dwell time in all non-zero

FRET states (Feldman et al., 2010). Kinetic parameters for conformational transitions were estimated from the dwell times observed in each state using the maximum interval likelihood algorithm implemented in QuB (QuB Suite, State University of New York, Buffalo, NY).

Puromycin reactivity assays

Puromycin assays were performed by stopped-flow delivery of neutralized puromycin (2 mM, pH 7.5) as previously described (Wang et al., 2011) in 80S Imaging Buffer to surface-immobilized ribosome complexes carrying Cy3-Met-$tRNA_i^{Met}$ in the P site on a MFK mRNA. Cy3-Met–Phe-$tRNA^{Phe}$ was generated in the A site by incubating surface-immobilized ribosomes with 50 nM eEF1A•GTP•Phe-$tRNA^{Phe}$ for 1 min before wash out. The loss of fluorescence over time, reporting on peptide release, was followed by strobe illumination at 5 mW laser power, taking a single, 100 ms frame every 20 s over a period of 20 min. The fluorescence intensity for each experiment was normalized to the total image intensity of the first frame.

Single-molecule tRNA selection assay

The process of tRNA selection on the ribosome was monitored using single-molecule FRET by stopped-flow injection of a 20 nM solution of ternary complex (eEF1A•GTP•aa-tRNA) containing (Cy5)Phe-$tRNA^{Phe}$ to surface-immobilized ribosome complexes containing (Cy3)$tRNA_i^{Met}$ in the P site, as previously described on a MFK mRNA (Geggier et al., 2010). Fluorescence signal was recorded at 200 mW laser illumination, 15 milliseconds exposure time per frame for 2000 frames. Processed and filtered traces were separated into individual events and post-synchronized to the first appearance of a FRET signal as described previously (Geggier et al., 2010). Each event was idealized using the segmental k-means algorithm and a model reflecting four distinct FRET states in analogy to the bacterial system (Geggier et al., 2010), which were identified by fitting a sum of four Gaussian functions to the histogram of observed FRET values. In order to generate FRET histograms representing complete accommodation of aa-tRNA into the A site, events that remained in a high (~ 0.69) FRET state (structurally assigned to the classical pre-translocation complex configuration) for at least 300 ms and lasted at least 2 s before photobleaching were selected. Transitions between states were summarized in a transition density plot by compiling the FRET values immediately before and after transitions into a two-dimensional histogram. PRE complex dynamics were analyzed as previously described (Budkevich et al. 2011).

The bimolecular rate constant of the initial interaction of eEF1a•GTP•aa-tRNA ternary complex with the ribosome was estimated in a two-step procedure. First, the stopped-flow mixing time in a given movie was determined by fitting a weighted sum of two exponential functions (assumed to represent mixing and photobleaching, respectively) to a plot of the observed background intensity in the darkest 25% of all pixels. Second, a histogram of the arrival times, i.e. the occurrence of the first data point with FRET ≥ 0.14, corrected for the mixing time, was generated and fit with a weighted sum of two exponential functions. The bimolecular rate constant was then estimated from the weighted sum of the decay rates, taking into account the known concentration of ternary complex.

Single-molecule translocation assay

Single-molecule translocation assays were adapted from (Munro et al., 2010c). Ribosome complexes carrying (Cy3)Met-$tRNA^{Met}$ in the P site on a MFK mRNA were surface-immobilized and (Cy5)Phe-$tRNA^{Phe}$ ternary complex was delivered to the A site to form a pre-translocation complex. eEF2 (2 μM), 1 mM GTP and 100 nM Cy5 dye (to mark the time of injection) were stopped-flow delivered. Fluorescence signal was recorded at 100 mW laser illumination, 40

milliseconds exposure time per frame for 2000 frames. Basic filtering criteria were the same as those used in the tRNA selection data analysis. The filtered traces were idealized using a five state hidden Markov model algorithm in QuB (QuB Suite, State University of New York, Buffalo, NY). Using this idealization, translocation traces and events were selected based on the transition from a low FRET state (0.17 ± 0.08 or 0.40 ± 0.08 idealized FRET efficiencies) into a high FRET state (0.64 ± 0.08 or 0.82 ± 0.08 idealized FRET efficiencies) followed by a high FRET state dwell time of 400 ms or longer (**Fig. 5**). Based on these criteria, cumulative distributions of translocation waiting times were produced which displayed bimodal behavior. Titration of eEF2 (**Fig. 5**) showed a Michaelis-Menten dependence of the fast mode rate of the distribution characterized by V_{max} = 8.93 ± 0.47 s^{-1} and K_M = 0.25 ± 0.05 μM, while the slow mode rate was approximately constant at 0.27 ± 0.05 s^{-1}. To generate a transition density plot (TDP), POST traces were idealized using a four state hidden Markov model algorithm in QuB. The analogous experiment performed on *E. coli* BL21 ribosomes was completed as described above with the substitution of EF-G (10 μM) in place of eEF2.

Single-molecule ribosomal exit (E) site stability assay

Ribosome complexes carrying (Cy3)Met-tRNA^{Met} in the P site on a MFF mRNA were immobilized as described above. The loss of Cy3 fluorescence over time, reporting on Cy3-labeled tRNA release, was followed by strobe illumination at 532nm, 5 mW laser power, taking a single 100 msec frame every 20 sec over a period of 20 min. PRE complexes were formed by delivery of a ternary complex (20 nM) containing eEF1A•GTP•(Cy5)Phe-tRNA^{Phe}. POST complexes were formed by incubating the PRE complex with eEF2 (200 nM)•GTP, as described above. eEF2 was rinsed out before stopped-flow addition of eEF1A•GTP•Phe-tRNA^{Phe} ternary complex to form PRE2. For the PRE2 plus eEF2 sample, eEF2•GTP and eEF1A•GTP•Phe-tRNA^{Phe} ternary complex were mixed and delivered in one single stopped-flow injection. Injections occurred just before the second imaging frame so that the first imaging frame contained 100% of the fluorescence signal and the fluorescence intensity for each experiment could be normalized to the total image intensity of the first frame. For analysis of 80S IC fluorescence, all molecules were assessed. For PRE, POST and PRE2 complexes, only molecules exhibiting FRET were considered in the analysis in order to eliminate 80S IC molecules that had not reacted. 80S IC, PRE and POST data were best fit by a single exponential decay process, as they were stable over the lifetime of the experiment and the slight loss of fluorescence could be attributed to photobleaching (~0.02 min^{-1} for all). PRE2 data were fit to double exponential decay processes with the equation $y = A_{fast}*\exp(-x/t_{fast}) + A_{slow}*\exp(-x/t_{slow})$ and reaction rates were calculated as the inverse of the population-weighted average of the two time constants.

Three-color single-molecule FRET imaging

Ribosome complexes carrying (Cy3)Met-tRNA^{Met} in the P site on a MFF mRNA were surface immobilized as described above. Three-color FRET imaging was performed as described in the sections “Single molecule fluorescence microscopy” and “Single-molecule FRET analysis”, with an additional camera to image Cy7-labeled tRNA in the A site. Fluorescence signal was recorded at 30 mW laser illumination, 200 milliseconds exposure time per frame for 2000 frames (Figure 5C, S5A; Figure 6, S6) or 100 mW laser illumination, 40 milliseconds exposure time per frame for 2000 frames (Figure S5B). Because the distance between Cy3-tRNA^{Met} in the E site and Cy7-tRNA^{Phe} in the A site is >100 Å (Budkevich et al., 2011), we expect negligible FRET efficiency between these fluorophores on the ribosome. With this simplifying approximation, FRET efficiency between E and P site tRNA (“E-P FRET”) can be calculated as $(I_5+I_7)/(I_3+I_5+I_7)$, where $I_3+I_5+I_7$ are the fluorescence intensities of Cy3, Cy5, and Cy7, respectively (Zhou and Ha, 2012).

FRET efficiency between the P and A site tRNAs ("P-A FRET") is then calculated as $I_7/(I_5+I_7)$. Both FRET signals are defined as zero when the donor fluorophore is dark and the total fluorescence intensity drops to the background levels. P-A FRET is defined as zero when Cy5 is dark and E-P FRET efficiency is below 0.2.

Quantification of ribosome conformation sub-state lifetimes

Processive translation reactions imaged using three-color single-molecule FRET were examined by visual inspection. The duration of functional states along the reaction coordinate were manually assigned through the identification of the characteristic signatures determined through single-turnover translation experiments. For PRE, characteristic fluctuations in Cy3-Cy5 FRET between 0.19, 0.37 and 0.69 FRET states were used as criteria. For POST, characteristic fluctuations in Cy3-Cy5 FRET between 0.35, 0.55 and 0.82 FRET states were used as criteria. Formation of the PRE2 complex was marked by start of Cy5-Cy7 FRET and increased Cy3-Cy5 FRET (~Δ0.04) that accompanies accommodation of the Cy7-labeled tRNA to the A site. The end of PRE2 lifetime was marked by the loss of Cy3 fluorescence and FRET.

SUPPLEMENTAL REFERENCES:

Ban, N., Beckmann, R., Cate, J. H. D., Dinman, J. D., Dragon, F., Ellis, S. R., et al. (2014). A new system for naming ribosomal proteins. *Current Opinion in Structural Biology*, 24, 165–169.

Bommer, U., Burkhardt, N., & Jünemann, R. (1997). Ribosomes and Polysomes. In Subcellular Fractionation : A Practical Approach, Graham, J. M. and Rickwood, D., ed. (Oxford, England: Oxford University Press), pp. 271-300.

Bunkenborg, J., García, G. E., Paz, M. I. P., Andersen, J. S., & Molina, H. (2010). The minotaur proteome: Avoiding cross-species identifications deriving from bovine serum in cell culture models. *Proteomics*, *10*(16), 3040–3044.

Cai, J., Wei, R., Ma, X., Zhu, H., & Li, Y. (2001). Cytotoxic effects of antiproliferative agents on human retinal glial cells in vitro. *International Ophthalmology*, *24*(4), 225–231.

Ha, T., Zhuang, X., Kim, H. D., Orr, J. W., Williamson, J. R., & Chu, S. (1999). Ligand-induced conformational changes observed in single RNA molecules. *Proceedings of the National Academy of Sciences*, *96*(16), 9077–9082.

Ingolia, N. T., Brar, G. A., Rouskin, S., McGeachy, A. M., & Weissman, J. S. (2012). The ribosome profiling strategy for monitoring translation in vivo by deep sequencing of ribosome-protected mRNA fragments. *Nature Protocols*, *7*(8), 1534–1550.

Grasmuk, H., Nolan, R.D., and Drews, J. (1977). Interchangeability of elongation factor-Tu and elongation factor-1 in aminoacyl-tRNA binding to 70 S and 80 S ribosomes. FEBS Lett. *82*, 237–242.

Käll, L., Canterbury, J. D., Weston, J., Noble, W. S., & MacCoss, M. J. (2007). Semi-supervised learning for peptide identification from shotgun proteomics datasets. *Nature Methods*, *4*(11), 923–925.

Kirillov, S. V., Makarov, E. M., & Semenkov YuP. (1983). Quantitative study of interaction of deacylated tRNA with Escherichia coli ribosomes. Role of 50 S subunits in formation of the E site. *FEBS Letters*, *157*(1), 91–94.

Krisko, I., Gordon, J., and Lipmann, F. (1969). Studies on the interchangeability of one of the mammalian and bacterial supernatant factors in protein biosynthesis. J. Biol. Chem. *244*, 6117–6123.

Langmead, B., & Salzberg, S. L. (2012). Fast gapped-read alignment with Bowtie 2. *Nature Methods*, *9*(4), 357–359.

McCann, J. J., Choi, U. B., Zheng, L., Weninger, K., & Bowen, M. E. (2010). Optimizing methods to recover absolute FRET efficiency from immobilized single molecules. *Biophysical Journal*, *99*(3), 961–970.

Qin, F. (2004). Restoration of single-channel currents using the segmental k-means method based on hidden Markov modeling. *Biophysical Journal*, *86*(3), 1488–1501.

Rashad, A. A., Mahalingam, S., & Keller, P. A. (2014). Chikungunya Virus: Emerging Targets and New Opportunities for Medicinal Chemistry. *Journal of Medicinal Chemistry*, *57*(4), 1147–1166.

Robinson, J. T., Thorvaldsdóttir, H., Winckler, W., Guttman, M., Lander, E. S., Getz, G., & Mesirov, J. P. (2011). Integrative genomics viewer. *Nature Biotechnology*, *29*(1), 24–26.

Zhou, R., and Ha, T. (2012). Single-molecule analysis of SSB dynamics on single-stranded DNA. *Methods Mol. Biol. 922*, 85–100.